RESEARCH ARTICLE | JANUARY 25 2007

# Comparison of electronic structures of $RuO_2$ and $IrO_2$ nanorods investigated by x-ray absorption and scanning photoelectron microscopy

H. M. Tsai; P. D. Babu; C. W. Pao; J. W. Chiou; J. C. Jan; K. P. Krishna Kumar; F. Z. Chien; W. F. Pong; M.-H. Tsai; C.-H. Chen; L. Y. Jang; J. F. Lee; R. S. Chen; Y. S. Huang; D. S. Tsai



*Appl. Phys. Lett.* 90, 042108 (2007)
https://doi.org/10.1063/1.2430929

# Comparison of electronic structures of $RuO_2$ and $IrO_2$ nanorods investigated by x-ray absorption and scanning photoelectron microscopy

H. M. Tsai, P. D. Babu,[a] C. W. Pao, J. W. Chiou, J. C. Jan, K. P. Krishna Kumar, F. Z. Chien, and W. F. Pong[b]
*Department of Physics, Tamkang University, Tamsui 251, Taiwan*

M.-H. Tsai
*Department of Physics, National Sun Yat-Sen University, Kaohsiung 804, Taiwan*

C.-H. Chen, L. Y. Jang, and J. F. Lee
*National Synchrotron Radiation Research Center, Hsinchu 300, Taiwan*

R. S. Chen and Y. S. Huang
*Department of Electrical Engineering, National Taiwan University of Science and Technology, Taipei 106, Taiwan*

D. S. Tsai
*Department of Chemical Engineering, National Taiwan University of Science and Technology, Taipei 106, Taiwan*

(Received 6 August 2006; accepted 8 December 2006; published online 25 January 2007)

Electronic structures of the nanorods of $RuO_2$ and $IrO_2$ metallic oxides were investigated by x-ray absorption near-edge structure (XANES) and scanning photoelectron microscopy (SPEM). O *K*-, Ru, and Ir $L_3$-edge XANES results reveal that hybridization between O $2p$ and metal $t_{2g}$ orbitals is weaker in $IrO_2$ than in $RuO_2$. The enhancement of the tip-region SPEM intensities relative to those in the sidewall regions for both $RuO_2$ and $IrO_2$ nanorods is found to extend over a large energy range in contrast to those of carbon nanotubes and ZnO nanorods, which are confined to deep below and near the Fermi level, respectively. © *2007 American Institute of Physics*.
[DOI: 10.1063/1.2430929]

One-dimensional (1D) nanomaterials, including nanorods, nanowires, and nanotubes, have attracted extensive attention because of their technological applications in nanodevices and fundamental scientific interest.[1–3] 1D nanomaterials with sharp tips of a high tip-height to base-diameter ratio are promising candidates for field emission applications.[4] Among various 1D nanostructures, carbon nanotubes (CNTs), which have been widely studied, exhibit excellent field emission properties with a low turn-on field. However, CNTs lack long-term stability, which is an important property for device applications.[4] Nanorods of metallic oxides such as $IrO_2$ and $RuO_2$ have recently been successfully synthesized. These oxides demonstrated to be potential candidates for use in field emission applications.[5,6] For instance, vertically aligned $IrO_2$ nanorods have been shown to exhibit excellent field emission characteristics that are comparable with those of CNTs and have a low turn-on field and more importantly the long-term stability.[5] The knowledge of their electronic structures is crucial in understanding field emission properties of these nanorods. The tips of nanotubes/nanorods of aligned CNTs (Ref. 7) and ZnO (Ref. 8) have recently been found to have enhanced electronic densities of states (DOSs). It is interesting to know whether $RuO_2$ and $IrO_2$ have similar enhancement of DOS's at the tips. Thus, the electronic structures of the nanorods of $RuO_2$ and $IrO_2$ metallic oxides have been investigated in this study by x-ray absorption near-edge structure (XANES) and scanning photoelectron microscopy (SPEM) measurements.

O *K*-, Ru, and Ir $L_3$-edge XANES and SPEM measurements were carried out at the National Synchrotron Radiation Research Center, Hsinchu, Taiwan. $RuO_2$ and $IrO_2$ nanorods were grown on a Si(100) substrate by chemical vapor deposition. Details of the preparation can be found elsewhere.[5,6] X-ray diffraction data presented in Fig. 1 show that $RuO_2$ and $IrO_2$ nanorods have a rutile structure and lattice constants agree with those reported in the literature. Scanning electron microscopy (SEM) images in insets (a) and (b) of Fig. 1 show nanorods with lengths (diameters) of ~700 nm (50–100 nm) and ~350 nm (50–70 nm) for $IrO_2$

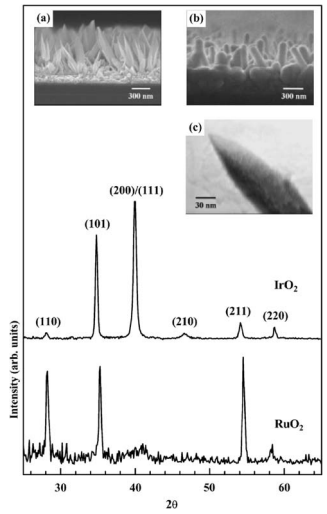


FIG. 1. X-ray diffraction patterns of $RuO_2$ and $IrO_2$ nanorods. Insets present SEM images of nanorods; (a) $IrO_2$, (b) $RuO_2$, and (c) TEM picture of the $IrO_2$ nanorod tip.

[a]On leave from: UGC-DAE Consortium for Scientific Research (formerly IUC-DAEF), Mumbai Center, BARC Campus Mumbai 400085, India.
[b]Author to whom correspondence should be addressed; electronic mail: wfpong@mail.tku.edu.tw



 

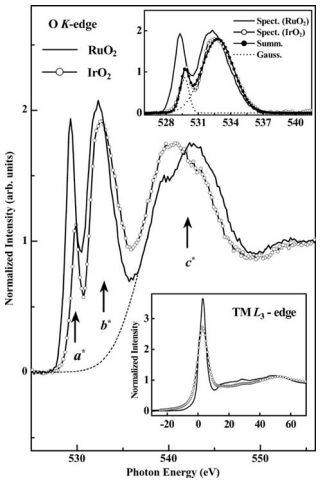


FIG. 2. O *K*-edge XANES spectra of $RuO_2$ and $IrO_2$ nanorods. Upper inset presents background corrected $\boldsymbol{a}^*$ and $\boldsymbol{b}^*$ features and the lower inset displays Ru and Ir $L_3$-edge XANES spectra.

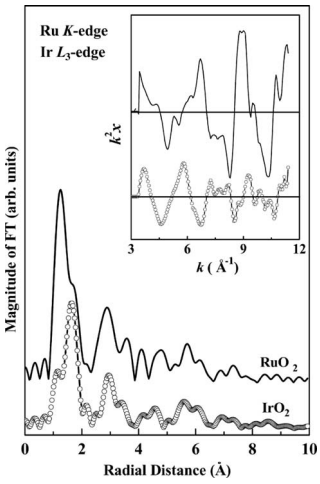


FIG. 3. Fourier transform spectra of EXAFS $k^2\chi$ data from $k=3.5$ 11.5 $Å^{-1}$ at Ru *K*- and Ir $L_3$-edge of $RuO_2$ and $IrO_2$ nanorods. Inset shows EXAFS $k^2\chi$ oscillations.

and $RuO_2$, respectively. Nanorods are more or less standing vertically though the alignment is not perfect. Transmission electron microscopy (TEM) reveals that $IrO_2$ nanorod tips displayed in the inset (c) of Fig. 1 are very sharp.

Figure 2 presents the normalized O *K*-edge XANES spectra of $RuO_2$ and $IrO_2$ nanorods. The O *K*-edge spectra of both $RuO_2$ and $IrO_2$ nanorods resemble closely with those of corresponding films, which were also collected as reference but not shown in the figure. The two sharp features denoted by $\boldsymbol{a}^*$ and $\boldsymbol{b}^*$ are attributable to the excitation of the O 1*s* core electrons into hybridized states between O 2*p* and Ru 4*d*/Ir $5dt_{2g}$ and $e_g$ states, respectively, due to splitting by the crystal field. The broad feature at higher energies denoted by $\boldsymbol{c}^*$ is due to excitation of core electrons into O 2*p* and Ru 5/Ir 6*sp* hybridized states. The intensity of the $t_{2g}$ ($\boldsymbol{a}^*$) feature is much lower for $IrO_2$ than for $RuO_2$. The upper inset magnifies $t_{2g}$ and $e_g$ ($\boldsymbol{a}^*$ and $\boldsymbol{b}^*$) features after background subtraction. The background is shown by a dashed line in the spectrum of $RuO_2$ as an example. The $t_{2g}$ and $e_g$ features in the spectra were deconvoluted by fitting two Gaussian profiles (represented by dotted lines shown in the upper inset for $IrO_2$ as an example). The area under each Gaussian curve gives the integrated intensity of the corresponding feature. The ranges of energies used to calculate integrated intensities of $t_{2g}$ and $e_g$ features are 527.5–530.9 and 527.5–537.5 eV for $RuO_2$, and 528.5–531.1 and 528.3–537.7 eV for $IrO_2$, respectively. The $t_{2g}/e_g$ intensity ratio decreases from ~0.29 for $RuO_2$ to ~0.12 for $IrO_2$ by a factor of ~2.4. The decrease is much greater than would be expected based on the electron count only. Assuming that $RuO_2$ and $IrO_2$ are 100% ionic, the tetravalent metal ions in $RuO_2$ and $IrO_2$ have four and five electrons left to fill 4*d* and 5*d* orbitals,[9] respectively. The $t_{2g}/e_g$ intensity ratio determined purely from the numbers of electrons needed to fill all 4*d* and 5*d* orbitals would decrease from 0.5 to 0.25 if one assumes that $e_g$ orbitals are completely empty. Note that under these assumptions the empty $t_{2g}$- and $e_g$-orbital number ratios are 2:4 (0.5) and 1:4 (0.25) for $RuO_2$ to $IrO_2$, respectively. This result indicates that $IrO_2$ has a lower degree of hybridization between O 2*p* and $t_{2g}$ orbitals than $RuO_2$ since other factors such as crystal structure and symmetry around O ions are similar. If the hybridization argument was right, the present O *K*-edge XANES result suggests that $RuO_2$ be more covalent than $IrO_2$, though Ru and Ir have electronegativity of 2.2.[10]

The lower inset in Fig. 2 displays the normalized Ru and Ir $L_3$-edge XANES spectra of $RuO_2$ and $IrO_2$ nanorods, respectively. The energy scale of the spectra in this figure was adjusted to match the peak positions and the zero energy corresponds to the absolute energies of 2842.4 and 11 217.4 eV in the Ru and Ir $L_3$-edge spectra, respectively. The sharp single peak corresponds to the electrons transition from the $2p_{3/2}$ level to unoccupied *d* (4*d* for $RuO_2$ and 5*d* for $IrO_2$) states.[11,12] The $t_{2g}$ and $e_g$ features are not resolved in these spectra. The smaller intensity of the $L_3$ white-line feature for $IrO_2$ reveals that the number of unoccupied metal 5*d* states in $IrO_2$ is smaller than that in $RuO_2$. Extended x-ray absorption fine structure (EXAFS) analyses at Ru *K* and Ir $L_3$ edges were performed to check for any difference in the local atomic structures in the two compounds. Figure 3 displays the Fourier transform (FT) of EXAFS $k^2\chi$ oscillations (shown in the inset). In general, the FT spectra of $RuO_2$ and $IrO_2$ nanorods are quite similar with those reported earlier,[13] indicating that the local atomic structures in $RuO_2$ and $IrO_2$ nanorods are similar to those of other materials with the rutile structure (such as $TiO_2$, $RuO_2$, and $IrO_2$ films/bulks). This implies that the local geometry around the absorbing atom is quite similar in $RuO_2$ and $IrO_2$ nanorods, so that differences in the XANES spectra of $RuO_2$ and $IrO_2$ nanorods are not due to different local atomic structures.

Figure 4 presents spatially resolved valence-band photoemission spectra (VB-PES) of the tip and sidewall regions of $RuO_2$ and $IrO_2$ nanorods. The upper insets show Ru 4*d* and Ir 5*d* SPEM cross-sectional images. The bright regions in the SPEM images correspond to the nanorods with maximum Ru 4*d* and Ir 5*d* intensities. Figure 4 displays the spectra, which show the photoelectron yields from the selected positions indicated in the images presented in the upper insets. These yields are the sum of (s1)–(s3) and (t1)–(t3) contributions from the sidewall and tip regions of $RuO_2$ and $IrO_2$ nanorods, respectively. The zero binding energy is set at the Fermi level, $E_F$, which is the threshold of the emission spectrum. The overall features of these PES are similar to the x-ray photoelectron spectra of bulk $RuO_2$ and $IrO_2$ reported previously.[14,15] The sharp features near/below $E_F$ denoted by *A* in the $RuO_2$ spectra and $A_1$ and $A_2$ in the $IrO_2$ spectra are basically associated with the *d* bands of metals. The splitting

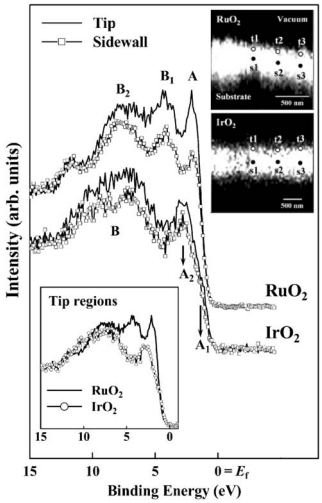


FIG. 4. Valence-band PES of $RuO_2$ and $IrO_2$ nanorods from selected regions of tips (t1)–(t3) and sidewalls (s1)–(s3), as displayed in SPEM images (upper insets). The lower inset compares PES data from the tip regions of $RuO_2$ and $IrO_2$ nanorods.

into features $A_1$ and $A_2$ was attributed to the spin-orbit effect.[9,14] The features denoted by $B$ in the $IrO_2$ spectra and $B_1$ and $B_2$ in the $RuO_2$ spectra correspond to the $\sigma$- and $\pi$-type molecular orbitals resulted from hybridization between O $2p$ and metal $d$ orbitals.[9,14] The lower inset compares tip-region PES data of both $RuO_2$ and $IrO_2$ nanorods. The PES data show that the Ir $d$ band is split into two subbands at ~1.1 eV ($A_1$) and ~2.5 eV ($A_2$) by the spin-orbit effect, whereas the Ru $d$ band has a single feature at ~2.1 eV ($A$). The VB-PES results at the first instance appear to contradict the XANES results since Ir has more $5d$ electrons than Ru in $4d$ and hence a larger PES intensity is expected for $IrO_2$ than $RuO_2$. This apparent contradiction is removed in the discussion below. In the vicinity of $E_F$, $RuO_2$ nanorods appear to have larger valence-band DOSs. Figure 4 clearly reveals that the valence-band DOSs in the tip regions is higher than those in the sidewall regions in both $RuO_2$ and $IrO_2$ nanorods. $RuO_2$ exhibits substantial enhancement of the near/below $E_F$ $d$-band PES intensity in the tip regions, whereas in the deeper O-$2p$/metal-$d$ region the PES intensity shows a relatively smaller increase in the tip regions. For $IrO_2$, however, the enhancement is relatively smaller for the entire valence band (features $A_1$, $A_2$, and $B$). The enhancement of valence-band DOSs at the tips is probably due to the increase of the number of dangling bonds and defects at the tips. These effects are also important in the sidewall regions as well but to a lower extent. The tips have much larger surface to volume ratio and the curvatures give rise further surface modification. This together with arguments presented below explains the larger PES intensity for $RuO_2$ than $IrO_2$.

A similar enhancement of the SPEM intensity has been observed previously at the tips of CNTs (Ref. 7) and ZnO nanorods.[8] In the case of CNTs, the enhancement of the intensity was observed at the energies more than 10 eV below $E_F$, which was argued to be caused by the alteration of the local electronic structure due to the curvature at the tip. As for ZnO nanorods, the enhancement of the intensity was observed only near/below $E_F$, which was argued to be associated with near-$E_F$ O $2p$ dangling-bond states.[8] The present results of the nanorods of metallic rutile oxides differ from those of CNTs and ZnO nanorods by that the enhancement of the valence-band DOSs extends from near $E_F$ down to approximately 10 eV below $E_F$, including both O $2p$ and metal $d$ states. The present results suggest that dangling bonds be not solely responsible for the enhancement because dangling-bond states lie near/below $E_F$ and are not expected to extend over such a large range of energies. $RuO_2$ and $IrO_2$ have a rutile structure, in which the metal atom is surrounded by an oxygen octahedron with six O ions. The coordination number of the metal atoms in $RuO_2$ and $IrO_2$ is larger than those in ZnO and the carbon atoms in CNTs. Thus, the termination at the tip is expected to yield more dangling bonds. Ru and Ir have the same electronegativity of 2.2,[10] which is much larger than that of Zn of 1.65. Thus, $RuO_2$ and $IrO_2$ are expected to contain a larger covalent character than ZnO, so that O $2p$ and Ru $4d/5sp$ and Ir $5d/6sp$ hybridization is expected to extend much deeper into the valence band than that of O $2p$ and Zn $3d/4sp$. Thus, the alteration of the coordination numbers and bonding arrangements of tip atoms affect even O $2p$ states deep in the valence band. The more significant enhancement of the tip-region PES intensity for $RuO_2$ nanorods than for $IrO_2$ nanorods can be attributable to their different tip shapes. The SEM pictures in the insets of Fig. 1 show that $RuO_2$ nanorods have round tips, while $IrO_2$ nanorods have pointlike tips, so that $RuO_2$ nanorods have a larger effective tip area and consequently a larger enhancement. The dangling bonds, defects, and other causes discussed above are also important in the nanorod sidewall region as well as the nanosized rods will have larger surface to volume ratio. However, their effect at tips is much more larger due to much larger surface to volume ratio and also due to curvature at the tips which give rise further surface modification. This together with arguments presented in previous paragraphs explains the larger PES intensity for $RuO_2$ than $IrO_2$.

This work was supported by the NSC of the ROC under Contract No. NSC 95-2112-M032-014.

[1] J. Hu, T. W. Odom, and C. M. Lieber, Acc. Chem. Res. **32**, 435 (1999).
[2] M. Law, J. Goldberger, and P. Yang, Annu. Rev. Mater. Res. **34**, 83 (2004).
[3] G. R. Patzke, F. Krumeich, and R. Nesper, Angew. Chem., Int. Ed. **41**, 2446 (2002).
[4] J. M. Bonard, J. P. Salvetat, T. Stockli, W. A. De Heer, L. Forro, and A. Chatelain, Appl. Phys. Lett. **73**, 918 (1998).
[5] R. S. Chen, Y. S. Huang, Y. M. Liang, C. S. Hsieh, D. S. Tsai, and K. K. Tiong, Appl. Phys. Lett. **84**, 1552 (2004).
[6] C. S. Hsieh, D. S. Tsai, R. S. Chen, and Y. S. Huang, Appl. Phys. Lett. **85**, 3860 (2004).
[7] J. W. Chiou, C. L. Yueh, J. C. Jan, H. M. Tsai, W. F. Pong, I. H. Hong, R. Klauser, M. H. Tsai, Y. K. Chang, Y. Y. Chen, C. T. Wu, K. H. Chen, S. L. Wei, C. Y. Wen, L. C. Chen, and T. J. Chuang, Appl. Phys. Lett. **81**, 4189 (2002).
[8] J. W. Chiou, J. C. Jan, H. M. Tsai, C. W. Bao, W. F. Pong, M. H. Tsai, I. H. Hong, R. Klauser, J. F. Lee, J. J. Wu, and S. C. Liu, Appl. Phys. Lett. **84**, 3462 (2004).
[9] L. F. Mattheiss, Phys. Rev. B **5**, 4219 (1972).
[10] *Table of Periodic Properties of the Elements* (Sargent-Welch, Skokie, IL, 1980).
[11] J. Stöhr and R. Jaeger, Phys. Rev. B **26**, 4111 (1982).
[12] G. Meitzner, G. H. Via, F. W. Lyte, and J. H. Sinfelt, J. Phys. Chem. **96**, 4960 (1992).
[13] T. Pauporte, D. Aberdam, J. L. Hazemann, R. Faure, and R. Duran, J. Electroanal. Chem. **465**, 88 (1999); W. Li, A. I. Frenkel, J. C. Woicik, C. Ni, and S. I. Shah, Phys. Rev. B **72**, 155315 (2005).
[14] R. R. Danels, G. Margaritondo, C. A. Georg, and F. Levy, Phys. Rev. B **29**, 1813 (1984).
[15] J. Riga, C. Tenret-Noël, J. J. Pireaux, R. Caudano, J. J. Verbist, and Y. Gobillon, Phys. Scr. **16**, 351 (1977).